IEEE Access
Multidisciplinary ⋮ Rapid Review ⋮ Open Access Journal

Received August 24, 2016, accepted September 7, 2016, date of publication October 18, 2016, date of current version November 18, 2016.

Digital Object Identifier 10.1109/ACCESS.2016.2616353

Joint Optimization of Energy Harvesting and Detection Threshold for Energy Harvesting Cognitive Radio Networks

GANGTAO HAN[1,2], JIAN-KANG ZHANG[2], (Senior Member, IEEE), AND XIAOMIN MU[1]
[1]School of Information Engineering, Zhengzhou University, Zhengzhou 450001, China
[2]Department of Electrical and Computer Engineering, McMaster University, Hamilton, ON L8S 4K1, Canada

Corresponding author: J.-K. Zhang (jkzhang@mail.ece.mcmaster.ca)

The work of G. Han and X. Mu was supported by the Natural Science Foundation of China under Grant 61271421, Grant 61301150, and Grant 61571401. The work of J.-K. Zhang was supported by NSERC.

ABSTRACT Spectrum efficiency and energy efficiency are two critical issues in the design of wireless communication networks. Recently, energy harvesting cognitive radio networks have been proposed to attempt to solve both the issues simultaneously. In this paper, we consider a cognitive radio network in which a primary transmitter mainly occupies the channel, and a secondary transmitter equipped with an energy harvesting device is allowed to opportunistically access the primary channel at any time if it is detected to be idle. Here, we assume that energy arrival process and primary channel state are random process and two-state time-homogenous discrete Markov process, respectively. Instead of the expected number of successful spectrum access attempts per time slot as a design criterion in current literature, we use the average channel capacity as the achievable throughput to jointly optimize energy harvesting and spectrum sensing subject to the constraints on the energy causality, collision, and temporal correlation of probability of sensing the idle/occupied channel, thus achieving or almost achieving both the energy efficiency and the spectrum efficiency in certain conditions. In addition, the corresponding optimum detection threshold and the maximum achievable throughput are obtained, which are substantiated by our comprehensive computer simulations.

INDEX TERMS Cognitive radio network, energy harvesting, spectrum sensing, achievable throughput, detection threshold.

I. INTRODUCTION

Recently, energy harvesting (EH) and opportunistic spectrum access have emerged as the promising solutions to improve energy efficiency and spectrum efficiency. On one hand, energy harvested from ambient sources (e.g., solar, wind, thermal, vibration, and even ambient radio power) can be utilized to improve the energy efficiency of wireless networks [1]–[4]. On the other hand, through dynamic spectrum access, cognitive radio networks (CRNs) can improve the spectrum efficiency and capacity of wireless networks [5]–[10]. Energy harvesting cognitive radio networks (EH-CRNs) which combine both of the EH and dynamic spectrum access techniques have received substantial attention [11]–[20]. In order to achieve both energy efficiency and spectral efficiency simultaneously for EH-CRNs, two fundamental constraints should be strictly satisfied, which are energy causality constraint and collision constraint [17]–[20]. Specifically, the energy causality constraint requires that the total consumed energy should not exceed the total harvested energy, and the collision constraint requires that the probability of accessing the occupied channel is less than or equal to the target probability of a collision with primary users.

Several energy harvesting wireless communication networks have been proposed to improve energy efficiency in the design of wireless communication networks. A mobile ad hoc network (MANET) powered by energy harvesting was proposed in [3], where transmitters were modelled as a homogeneous Poisson point process (PPP). By applying the random-walk theory, it was proved that transmission probability was equal to the smaller of one and the ratio between the energy-arrival rate and transmission power, and meanwhile, the maximum space throughput was proportional to the optimal transmission probability. In [21], a general system model consisting of K classes of self-powered base stations (BSs) was developed, which modelled the temporal dynamics of the energy level at each BS as a birth-death process and an energy utilization rate was derived. A harvest-use-store architecture for energy harvesting wireless systems was reported in [13], in which the harvested energy was used to data transmission first and then stored in the storage device while there was surplus.

In addition, there are some other works on EH-CRNs proposed to achieve both energy efficiency and spectral efficiency simultaneously. In [12], both the transmission probability of secondary transmitters and the outage probability of the primary receivers and secondary receivers were analyzed, where primary transmitters and secondary transmitters were considered to be distributed as independent homogeneous Poisson point processes (HPPPs) and communicated with their intended receivers at fixed distances, and the optimal transmission power and density of secondary transmitters were derived for maximizing the secondary network spatial throughput when the secondary transmitters harvested ambient radio frequency energy from transmissions by nearby active primary transmitters. The optimal cognitive sensing and access policies for a secondary user was investigated in [16], which was formulated as a Markov decision process (MDP). The optimal channel selection policy for the secondary user was studied in [22] to select one of the channels to transmit data when it was idle, and to harvest radio frequency energy when the primary user was transmitting data. A saving-sensing-transmitting structure was studied in [23], where the expected achievable throughput of secondary user was formulated as a mixed integer nonlinear programming (MINLP) problem over all of the idle channels in one time slot. In [24], sensing strategy and power allocation strategy were jointly considered to maximize the throughput of secondary user over multiple consecutive time slots, and a sub-optimal online algorithm was proposed based on the dynamic spectrum state, harvested energy, and the channel fading level. Recently, by splitting the EH-CRNs [17]–[20] into a spectrum-limited regime and an energy-limited regime, an optimal detection threshold to maximize the expected number of successful spectrum access attempts per time slot of secondary user was derived under energy causality and collision constraints in [17] and then, the optimal sensing decision policy and access policy were formulated as a constrained partially observable Markov decision process (POMDP) in [18], and a sub-optimal myopic policy was proposed. Furthermore, the relationship between the optimal sensing duration and the corresponding detection threshold in order to maximize the average throughput was studied subject to the energy causality and collision constraints in [19]. Besides, the primary traffic was modeled as a time-homogeneous discrete Markov process in [20], and the upper bound on expected number of successful spectrum access attempts per time slot of secondary user was derived. Nevertheless, the study on EH-CRNs is not sufficient, and there is still a lot of work to do.

In this paper, we use the average channel capacity as the achievable throughput instead of the expected number of successful spectrum access attempts per time slot as in [20]. In addition, we treat the energy harvesting rate as an optimization variable, since the optimal energy harvesting rate is fixed for the given detection threshold under these constraints, and hence, higher energy harvesting rate will not improve the spectrum efficiency. The harvested energy overflowing the optimal energy harvesting rate can be used for other purpose. Therefore, our objective function and constraints are different from [20]. Aiming to attempt to achieve both the energy efficiency and the spectrum efficiency, joint optimization problem of energy harvesting and spectrum sensing is studied under the energy causality constraint, collision constraint and temporal correlation constraints of probability of sensing the idle/occupied channel. By making use of the feature of both the objective function and the constraints, our idea is to solve the optimization problem for any allowably fixed energy harvesting rate and detection threshold, to first maximize the objective function with respect to the design variables probability of sensing the idle/occupied channel, and then, to maximize the resulting objection function with respect to the design variables energy harvesting rate and detection threshold. Finally, the optimal energy harvesting rate and detection threshold are derived, and the effect of target collision probability and the temporal correlation constraint of sensing the idle/occupied channel on the achievable throughput are also discussed.

The remainder of this paper is organized as follows: The primary network and cognitive radio network models are described in Section II. The joint optimization problem of detection threshold and energy harvesting to maximize the achievable throughput of secondary user is formulated in Section III, in which the optimal detection threshold and the maximum achievable throughput of the energy harvesting secondary transmitter subject to the energy causality and collision constraints is derived and the optimal detection threshold is also studied while the energy harvesting rate is under the optimal value. Finally, numerical results are provided in Section IV, and our conclusions are presented in Section V.

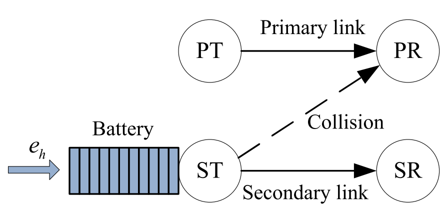

FIGURE 1. System model.

II. ENERGY HARVESTING COGNITIVE RADIO SYSTEMS MODEL

In this section, we are interested in a simple EH-CRN consisting of one primary link and one secondary link [17], as shown in Fig. 1, in which the secondary transmitter is equipped with an energy harvesting device and an infinite-capacity rechargeable battery. For such a system, we assume that harvested energy will be stored in the rechargeable battery before it is used, and that it is possible for secondary user to opportunistically access the primary channel if it is detected idle. We also assume there is always data for secondary user to transmit and the communication system is operated in a time-slotted model. In the following, a primary network model is briefly reviewed, followed by the description of cognitive radio network with spectrum sensing and energy harvesting model.

A. PRIMARY NETWORK MODEL

By assuming the primary user employs a time-slotted network model with duration T and bandwidth W, a primary channel occupation state is modeled as a two-state time-homogenous discrete Markov process. A channel occupation state in slot n is denoted by $S_n \triangleq \{0(\text{idle}), 1(\text{occupied})\}$, the probability of transit from state 0 to itself is q_i, and the probability of transit from state 1 to itself is q_o. Then, the steady-state probabilities of spectrum being idle and occupied are given by $\pi_i = \frac{1-q_o}{2-q_i-q_o}$ and $\pi_o = \frac{1-q_i}{2-q_i-q_o}$, respectively. In addition, we assume that the secondary transmitter is aware of the state transition probabilities through long-term channel usage measurements [20].

B. COGNITIVE RADIO NETWORK MODEL

1) SPECTRUM SENSING

The secondary link is assumed to be comprised of an energy harvesting secondary transmitter and an energy unconstrained secondary receiver. Assuming that it always has data to be transmitted, the secondary transmitter periodically executes spectrum sensing with slot duration T, which is divided into a sensing phase with duration τ and a transmission phase with duration $T - \tau$. The presence of a primary user is detected through a binary hypothesis test:

$$y_n(m) = \begin{cases} w(m), & \mathcal{H}_0 \quad (1a) \\ s(m) + w(m), & \mathcal{H}_1, \quad (1b) \end{cases}$$

where $\mathcal{H}_0$ and $\mathcal{H}_1$ mean that primary channel is in idle and occupied state, respectively, $y_n(m)$ is the m-th sample of the secondary transmitter energy detector in a slot n, $s(m)$ and $w(m)$ are the primary transmitter signal and noise, respectively, and they are both assumed to be independent circularly symmetric complex Gaussian (CSCG) random processes with respective variances σ_p^2 and σ_w^2. If we let f represent a sampling frequency, then, the number of samples is τf. When τf is large enough, the probability of false alarm $P_f(\varepsilon)$ and the probability of detection $P_d(\varepsilon)$ are given by [25]

$$P_f(\varepsilon) = \mathcal{Q}\left(\left(\frac{\varepsilon}{\sigma_w^2} - 1\right)\sqrt{\tau f} \right), \tag{2}$$

$$P_d(\varepsilon) = \mathcal{Q}\left(\left(\frac{\varepsilon}{(\sigma_w^2 + \sigma_p^2)} - 1\right)\sqrt{\tau f} \right), \tag{3}$$

where $\varepsilon \in \mathbb{R}_+$ denotes a detection threshold for the energy detector and $\mathcal{Q}(x) \triangleq \frac{1}{\sqrt{2\pi}} \int_x^\infty \exp\left(-\frac{u^2}{2}\right) du$. After spectrum sensing in slot n, the detection result is denoted as $\theta_n \triangleq \{0(\text{idle}), 1(\text{occupied})\}$.

2) ENERGY HARVESTING MODEL

Here, the harvested energy arrives randomly in each slot and is stored in a rechargeable battery of infinite capacity. We model the energy arrival process $\{E_n^h\} \subset \mathbb{R}_+$ as an i.i.d. random process with mean $\mathbb{E}[E_n^h] = e_h$, where e_h is actually the energy arrival rate as well as the energy harvesting rate. The energy consumption of the secondary transmitter during slot n is given by $E_n^c(\theta_n) = e_s + (1-\theta_n)e_t$, where $e_s = \tau P_s \in \mathbb{R}_+$ is the energy consumed during spectrum sensing phase, P_s is the sensing power, and $e_t = (T-\tau)(\frac{\xi}{\zeta}P_t + P_c) \in \mathbb{R}_+$ is the energy consumed in the data transmitting phase, with P_t being the transmission power, ξ being the peak-to-average ratio (PAR) of the power amplifier (PA), ζ being the drain efficiency of the PA, and P_c being the power consumed in various transmitter and receiver electronic circuits, excluding the PA power [26].

III. JOINT OPTIMIZATION OF HARVESTED ENERGY AND SENSING THRESHOLD

Our primary purpose in this section is to use the average channel capacity as the achievable throughput for jointly optimizing energy harvesting and spectrum sensing. To do this, let us first introduce the definition of the probability of sensing the idle/occupied channel.

A. PROBABILITY OF SENSING THE IDLE/OCCUPIED CHANNEL

$P_i \triangleq Pr(active|\mathcal{H}_0)$ and $P_o \triangleq Pr(active|\mathcal{H}_1)$ are defined as the probabilities that the secondary transmitter will select the active mode to execute spectrum sensing while the primary channel is idle or occupied, respectively, under any spectrum access policy for given energy harvesting rate e_h and detection threshold ε [20].

Normally, when optimizing energy harvesting and spectrum sensing, we need to consider the following three constraints:

B. ENERGY CAUSALITY CONSTRAINT

It is required that energy can not be consumed before it is harvested, which means $E_n^c \le E_n^h$ in each slot. Since the capacity of the battery is assumed to be infinite, the harvested energy that can not be consumed in each slot will be stored in the battery for further use. From the long term operation perspective, we obtain the energy causality constraint:

$$E_i^c(\varepsilon)P_i + E_o^c(\varepsilon)P_o \le e_h, \tag{4}$$

where $E_i^c(\varepsilon) = \big(e_s + \big(1 - P_f(\varepsilon)\big)e_t\big)\pi_i$ and $E_o^c(\varepsilon) = \big(e_s + \big(1 - P_d(\varepsilon)\big)e_t\big)\pi_o$ are the expectation of energy consumption during an idle/occupied slot of the secondary transmitter, respectively [20].

C. COLLISION CONSTRAINT

It requires the probability of accessing the occupied channel is less than or equal to the target collision probability, which is expressed as:

$$P_o\big(1 - P_d(\varepsilon)\big) \le P_{col}, \tag{5}$$

where P_{col} is the target collision probability that the primary user can tolerate.

D. TEMPORAL CORRELATION CONSTRAINTS OF PROBABILITY OF SENSING THE IDLE/OCCUPIED CHANNEL

$$\alpha P_i \le P_o \le \beta P_i, \tag{6}$$

where

$$\alpha = \max\left(\frac{1-\max(1-q_o, q_i)}{\max(1-q_o, q_i)}, \frac{\min(1-q_i, q_o)}{1-\min(1-q_i, q_o)}\right) \times \frac{1-q_o}{1-q_i}, \tag{7}$$

$$\beta = \min\left(\frac{1-\min(1-q_o, q_i)}{\min(1-q_o, q_i)}, \frac{\max(1-q_i, q_o)}{1-\max(1-q_i, q_o)}\right) \times \frac{1-q_o}{1-q_i}. \tag{8}$$

The derivations of (6), (7) and (8) are provided in [20].

There are two scenarios under which the secondary network can operate in the primary channel.

- Scenario I: When the primary channel is idle ($\mathcal{H}_0$) and the detection result is $\theta_n = 0$, the achievable throughput of the secondary link is $\frac{T-\tau}{T}C_i$, and the probability of this scenario is given by $P_i(1 - P_f(\varepsilon))\pi_i$.
- Scenario II: When the primary channel is occupied ($\mathcal{H}_1$) and the detection result is $\theta_n = 0$, the achievable throughput of the secondary link is $\frac{T-\tau}{T}C_o$, and the probability of this scenario is determined by $P_o\big(1-P_d(\varepsilon)\big)\pi_o$.

As a result, the average throughput for the secondary network is determined by [25]

$$R(P_i, P_o, e_h, \varepsilon) = \Phi_i P_i\big(1-P_f(\varepsilon)\big) + \Phi_o P_o\big(1-P_d(\varepsilon)\big), \tag{9}$$

where $\Phi_i = \frac{T-\tau}{T}C_i\pi_i$, $\Phi_o = \frac{T-\tau}{T}C_o\pi_o$, $C_i = W\log(1+\gamma_s)$, $C_o = W\log(1+\frac{\gamma_s}{1+\gamma_p})$, and γ_s and γ_p are received signal-to-noise ratio (SNR) of secondary signal and primary signal at the secondary network, respectively.

Therefore, our objective in this paper is to find the optimum detection threshold ε, energy harvesting rate e_h and probabilities of sensing the Idle/occupied channel for maximizing the throughput of the EH-CRN, i.e.,

Problem 1: Find the probabilities of sensing the idle/occupied channel, the energy arrival rate and the detection threshold such that

$$\begin{aligned} &\max_{P_i, P_o, e_h, \varepsilon} \; R(P_i, P_o, e_h, \varepsilon), \\ &s.t. \; E_i^c(\varepsilon)P_i + E_o^c(\varepsilon)P_o \le e_h, \\ &\qquad P_o\big(1-P_d(\varepsilon)\big) \le P_{col}, \\ &\qquad \alpha P_i \le P_o \le \beta P_i. \end{aligned} \tag{10}$$

■

In order to efficiently solve Problem 1, we need to investigate the effect of probability of sensing the idle/occupided channel on the achievable throughput for any given energy harvesting rate and detection threshold. By making use of the feature of both the objective function and the constraints, our idea to solve Problem 1 is for any allowably fixed e_h and ε, to first maximize the objective function with respect to the design variables P_i and P_o, and then, to solve the resulting optimization problem with respect to the variables e_h and ε. To do that, we need to first establish the following lemma:

Lemma 1: Let $R(e_h, \varepsilon) = \max_{P_i, P_o} R(P_i, P_o, e_h, \varepsilon)$. Then, the following two statements are true.

1) If $\alpha > P_{col}$, we have

$$R(e_h, \varepsilon) = \begin{cases} \Phi_i\big(1-P_f(\varepsilon)\big) + \Phi_o\big(1-P_d(\varepsilon)\big), & (e_h, \varepsilon) \in \Omega_1; \\ \Phi_i\big(1-P_f(\varepsilon)\big) + \Phi_o P_{col}, & (e_h, \varepsilon) \in \Omega_2; \\ \Phi_i \frac{P_{col}\big(1-P_f(\varepsilon)\big)}{\alpha\big(1-P_d(\varepsilon)\big)} + \Phi_o P_{col}, & (e_h, \varepsilon) \in \Omega_3; \\ \Phi_i\big(1-P_f(\varepsilon)\big) + \Phi_o \mu(e_h, \varepsilon)\big(1-P_d(\varepsilon)\big), & (e_h, \varepsilon) \in \Omega_4; \\ \lambda(e_h, \varepsilon)\Big(\Phi_i\big(1-P_f(\varepsilon)\big) + \Phi_o\alpha\big(1-P_d(\varepsilon)\big)\Big), & (e_h, \varepsilon) \in \Omega_5. \end{cases} \tag{11}$$

where $\mu(e_h, \varepsilon) = \big(e_h - E_i^c(\varepsilon)\big)/E_o^c(\varepsilon)$, $\lambda(e_h, \varepsilon) = e_h/\big(E_i^c(\varepsilon) + \alpha E_o^c(\varepsilon)\big)$, and

$$\Omega_1 = \Big\{(e_h, \varepsilon) | \mu(e_h, \varepsilon) \ge 1, \frac{P_{col}}{1-P_d(\varepsilon)} \ge 1\Big\},$$

$$\Omega_2 = \Big\{(e_h, \varepsilon) | \alpha \le \frac{P_{col}}{1-P_d(\varepsilon)} < \min\big(1, \mu(e_h, \varepsilon)\big)\Big\},$$

$$\Omega_3 = \Big\{(e_h, \varepsilon) | \frac{P_{col}}{1-P_d(\varepsilon)} < \alpha \min\big(1, \lambda(e_h, \varepsilon)\big)\Big\},$$

$$\Omega_4 = \Big\{(e_h, \varepsilon) | \alpha \le \mu(e_h, \varepsilon) < \min\big(1, \frac{P_{col}}{1-P_d(\varepsilon)}\big)\Big\},$$

$$\Omega_5 = \Big\{(e_h, \varepsilon) | \lambda(e_h, \varepsilon) \le \min\big(1, \frac{P_{col}}{\alpha(1-P_d(\varepsilon))}\big)\Big\}.$$

2) If $\alpha \le P_{col}$, we have

$$R(e_h, \varepsilon) = \begin{cases} \Phi_i\big(1-P_f(\varepsilon)\big) + \Phi_o\big(1-P_d(\varepsilon)\big), & (e_h, \varepsilon) \in \Omega_1; \\ \Phi_i\big(1-P_f(\varepsilon)\big) + \Phi_o P_{col}, & (e_h, \varepsilon) \in \bar{\Omega}_2; \\ \Phi_i\big(1-P_f(\varepsilon)\big) + \Phi_o \mu(e_h, \varepsilon)\big(1-P_d(\varepsilon)\big), & (e_h, \varepsilon) \in \Omega_4; \\ \lambda(e_h, \varepsilon)\big(\Phi_i(1-P_f(\varepsilon)) + \Phi_o\alpha(1-P_d(\varepsilon))\big), & (e_h, \varepsilon) \in \bar{\Omega}_5. \end{cases} \tag{12}$$

where $\bar{\Omega}_2 = \big\{(e_h, \varepsilon) | \frac{P_{col}}{1-P_d(\varepsilon)} < \min\big(1, \mu(e_h, \varepsilon)\big)\big\}$, $\bar{\Omega}_5 = \big\{(e_h, \varepsilon) | \lambda(e_h, \varepsilon) \le 1\big\}$. ■

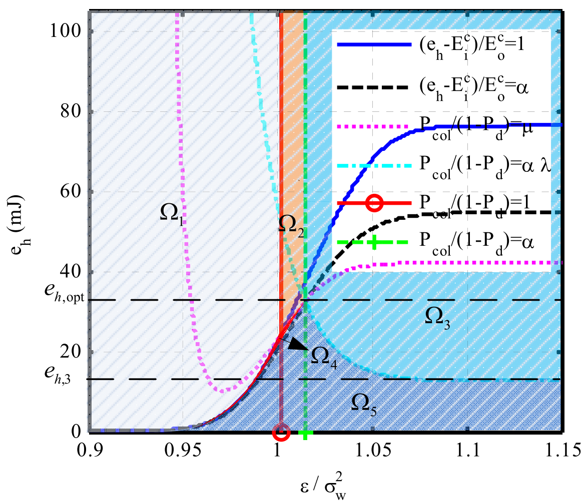

FIGURE 2. Distribution of (e_h, ε) while $\alpha > P_{col}$.

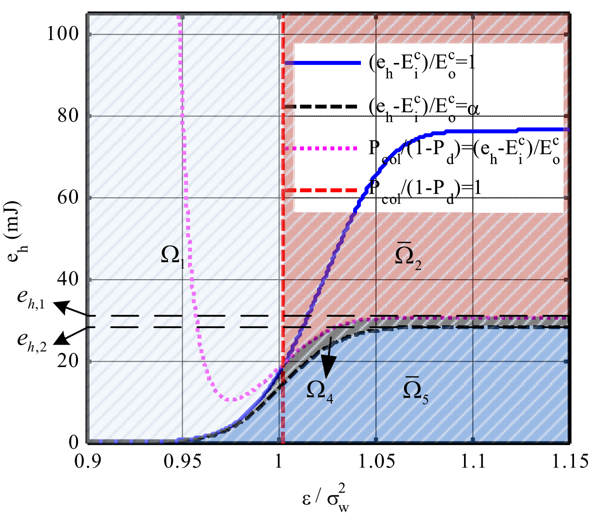

FIGURE 3. Distribution of (e_h, ε) while $\alpha \le P_{col}$.

The proof of Lemma 1 is given in Appendix A. To make Lemma 1 understandable more clearly, the feasible domain of (e_h, ε) is shown in Figs. 2 and 3, in which the parameters e_h and ε of $P_d(\varepsilon), E_i^c(\varepsilon), E_o^c(\varepsilon), \mu(e_h, \varepsilon), \lambda(e_h, \varepsilon)$ are omitted for simplicity. We can see from Lemma 1 that the feasible set of (e_h, ε) to maximize the achievable throughput is divided into five regions if $\alpha > P_{col}$ and four regions if $\alpha \le P_{col}$. There are different expressions for the achievable throughput in each region of (e_h, ε), and each of them is a continuous function at the edge between adjacent regions. To further maximize $R(e_h, \varepsilon)$, let us study the monotonicity property in each region. We need to establish the following lemma.

Lemma 2: Let $F(\varepsilon) = 1 - P_f(\varepsilon) - \frac{P_f'(\varepsilon)}{P_d'(\varepsilon)}\big(1 - P_d(\varepsilon)\big)$. Then, there exists such $\tilde{\varepsilon} \in \big(\frac{\sigma_w^2(\sigma_w^2+\sigma_p^2)}{\sigma_p^2+2\sigma_w^2}, \sigma_w^2 + \sigma_p^2\big)$ that $F(\varepsilon) < 0$ if $\varepsilon < \tilde{\varepsilon}$ and $F(\varepsilon) > 0$ if $\varepsilon > \tilde{\varepsilon}$. ■

The proof is postponed to Appendix B. After having all the above preparations, we are now in a position to formally state our main result in this paper.

Theorem 1: The solution to Problem 1 is given below:

1) If $\alpha > P_{col}$, we have $\varepsilon_{opt} = (\mathcal{Q}^{-1}(1 - \frac{P_{col}}{\alpha})/\sqrt{\tau f} + 1)(\sigma_w^2 + \sigma_p^2)$, $e_{h,opt} = E_i^c(\varepsilon_{opt}) + \alpha E_o^c(\varepsilon_{opt})$, $P_{i,opt} = 1$ and $P_{o,opt} = P_{col}/(1 - P_d(\varepsilon_{opt}))$. In addition, the resulting maximum value is given by

$$R(P_{i,opt}, P_{o,opt}, e_h, \varepsilon_{opt}) = \Phi_i\big(1 - P_f(\varepsilon_{opt})\big) + \Phi_o P_{col}.$$

for any $e_h \ge e_{h,opt}$.

2) If $\alpha \le P_{col}$, we have $R(P_i, P_o, e_h, \varepsilon) < \Phi_i + \Phi_o P_{col}$. Furthermore, we can obtain

$$\lim_{\varepsilon\to\infty} R(1, P_{col}, e_h, \varepsilon) = \Phi_i + \Phi_o P_{col}.$$

for any $e_h \ge e_{h,1}$, where $e_{h,1} = (e_s + e_t)(\pi_i + P_{col}\pi_o)$. ■

The proof of Theorem 1 is provided in Appendix C. To make Theorem 1 more understandable, Figs. 4 and 5 are plotted to show the achievable throughput for $\alpha > P_{col}$ and $\alpha \le P_{col}$, respectively. From Fig. 4, it can be seen that the throughput achieves maximum at ε_{opt} and $e_h \in [e_{h,opt}, \infty)$. In addition, it can be also observed from Fig. 5 that $R(e_h, \varepsilon)$ is an increasing function in terms of ε for $e_h \ge e_{h,1}$ and exponentially approaches to the upper bound $\Phi_i + \Phi_o P_{col}$, i.e., limit. In fact, we find that $R(e_h, \varepsilon)$ keeps almost unchanged when $\varepsilon \ge 1.15\sigma_w^2$. Hence, the limit of the throughput can be approximately treated as the maximum achievable throughput at $\varepsilon \approx 1.15\sigma_w^2$.

However, in some practical environments where the energy harvesting rate is fixed. Therefore, instead of totally optimizing the throughput in Problem 1, we now consider to optimize the throughput subject to the optimal probabilities of sensing the idle/occupied channel, as suggested by Lemma 1, and a fixed energy harvesting rate, i.e., find a detection threshold such that $R(P_{i,opt}, P_{o,opt}, e_h, \varepsilon)$ can be made as large as possible when the primary signal SNR is low.

Theorem 2: The following statements are true.

1) $\alpha > P_{col}$. If $e_h \in [e_{h,3}, e_{h,opt})$, $e_{h,3} = \frac{1}{\alpha}(e_s + e_t)(\pi_i + \alpha\pi_o)P_{col}$, then, the maximum $R(e_h, \varepsilon)$ with respect to ε is given by

$$R(e_h, \varepsilon_{opt,2}) = \Phi_i \frac{P_{col}(1 - P_f(\varepsilon_{opt,2}))}{\alpha(1 - P_d(\varepsilon_{opt,2}))} + \Phi_o P_{col}$$

with $\varepsilon_{opt,2} = Y^{-1}(0)$, where $Y^{-1}(\varepsilon)$ denotes the inverse function of $Y(\varepsilon) = \lambda(e_h, \varepsilon) - \frac{P_{col}}{\alpha(1-P_d(\varepsilon))}$.
If $e_h \in (0, e_{h,3})$, then, we have $R(e_h, \varepsilon) < \frac{e_h(\Phi_i+\alpha\Phi_o)}{(e_s+e_t)(\pi_i+\alpha\pi_o)}$, and furthermore,

$$\lim_{\varepsilon\to\infty} R(e_h, \varepsilon) = \frac{e_h(\Phi_i + \alpha\Phi_o)}{(e_s + e_t)(\pi_i + \alpha\pi_o)}.$$

2) $\alpha \le P_{col}$. In this case, if $e_h \in [e_{h,2}, e_{h,1})$, $e_{h,2} = (e_s + e_t)(\pi_i + \alpha\pi_o)$, then, we attain

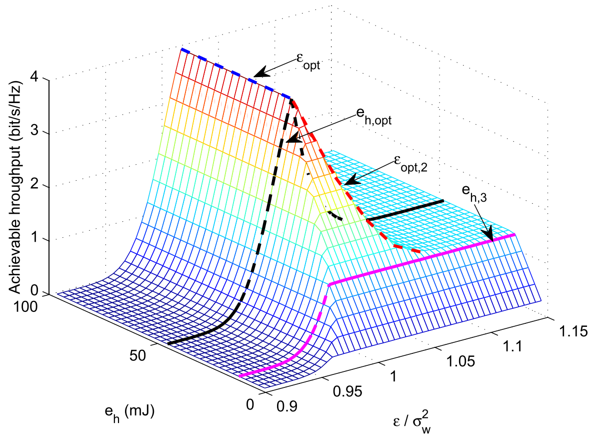

FIGURE 4. The maximum achievable throughput vs detection threshold and energy harvesting rate while $\alpha > P_{col}$.

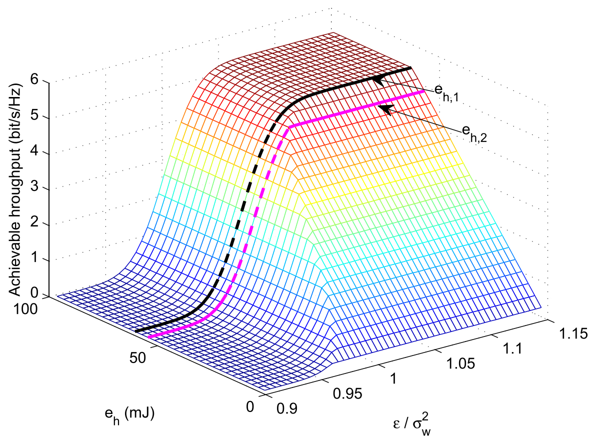

FIGURE 5. The maximum achievable throughput vs detection threshold and energy harvesting rate while $\alpha \leq P_{col}$.

$R(e_h, \varepsilon) < \Phi_i + \Phi_o\left(\frac{e_h}{(e_s+e_t)\pi_o} - \frac{\pi_i}{\pi_o}\right)$, and

$$\lim_{\varepsilon\to\infty} R(e_h, \varepsilon) = \Phi_i + \Phi_o\left(\frac{e_h}{(e_s + e_t)\pi_o} - \frac{\pi_i}{\pi_o}\right).$$

If $e_h \in (0, e_{h,2})$, then, we obtain $R(e_h, \varepsilon) < \frac{e_h(\Phi_i+\alpha\Phi_o)}{(e_s+e_t)(\pi_i+\alpha\pi_o)}$, and

$$\lim_{\varepsilon\to\infty} R(e_h, \varepsilon) = \frac{e_h(\Phi_i + \alpha\Phi_o)}{(e_s + e_t)(\pi_i + \alpha\pi_o)}.$$

■

The proof of Theorem 2 is given in Appendix D. Some observations similar to Theorem 1 can be also made for Theorem 2 from Figs. 4 and 5. Specifically, we can see from Fig. 4 that the throughput increases with ε increasing and exponentially approaches to the limit when $e_h < e_{h,3}$. However, when $e_h \in [e_{h,3}, e_{h,opt})$, there is an optimal detection threshold to maximize the throughput. From Fig. 5, we can also see that the throughput increases with ε increasing and exponentially approaches to the limit when $e_h < e_{h_1}$. From both figures, we can observe that $R(e_h, \varepsilon)$ keeps almost unchanged when $\varepsilon \geq 1.15\sigma_w^2$. Hence, the limits in Theorem 2 can also be approximately regarded as the maximum achievable throughput in practice.

IV. NUMERICAL RESULTS

In this section, the performance of the proposed schemes are presented through computer simulations (MATLAB). The system parameters are summarized in Table 1, which is mainly drawn from [20].

TABLE 1. Value of parameters in numerical result.

W	Bandwidth	1 MHz
P_s	Sensing Power	110 mW
pt	Transmission power	50 mW
P_c	Circuit power	210 mW
ξ	Peak-to-average ratio of PA	6 dB
ζ	Drain efficiency	0.35
T	Slot length	100 ms
τ	Sensing duration	2 ms
π_i	Prob. of being idle state	0.8
γ_p	Primary SNR	-15 dB
γ_s	Secondary SNR	20 dB
$P_{\rm col}$	Target collision probability	0.1
f	Sampling frequency	1 MHz

Fig. 4 shows the maximum achievable throughput of secondary user for $\alpha > P_{col}$ where $q_i = 0.9$, $q_o = 0.6$, $\alpha = 0.4444$. Fig. 5 shows the condition that $\alpha \leq P_{col}$, where $q_i = 0.9875$, $q_o = 0.95$, $\alpha = 0.0506$. From Fig. 4, it can be observed that the achievable throughput increases with e_h before it reaches the optimal value, and then, it keeps unchanged, since the harvested energy is sufficient to occupy all the opportunity to implement data transmitting under the collision constraint. It can be also observed that the achievable throughput increases with ε when $e_h \geq e_{h,opt}$, and decreases with ε after it obtains the optimal ε, which means that P_f is high when ε is small and most of the opportunities to access the primary channel is missed, resulting in low throughput. On the other hand, with ε increasing, more collision will happen and thus, the achievable throughput decreases. In addition, we can see that there is no optimal ε when $\alpha \leq P_{col}$, as shown in Fig. 5, which means that secondary user can access the primary channel as long as the probability of secondary user accessing the occupied primary channel is not larger than the target collision probability and hence, there is no need to operate spectrum sensing.

Fig. 6 depicts the optimal energy harvesting rate to achieve the maximum achievable throughput of EH-CRNs for different π_i and α. For discussion convenience, $e_{h,1}$ is also called the optimal energy harvesting rate for the case of $\alpha \leq P_{col}$. From the figure we can see that the optimal e_h to achieve the maximum achievable throughput increases with π_i, and increases as α decreases before $\alpha = P_{col}$, and then, keeps unchanged when $\alpha < P_{col}$. On one hand, since the secondary user can obtain more spectrum access opportunities with π_i increasing, more energy is needed to execute data processing and transmission. On the other hand, if $\alpha > P_{col}$, ε_{opt}

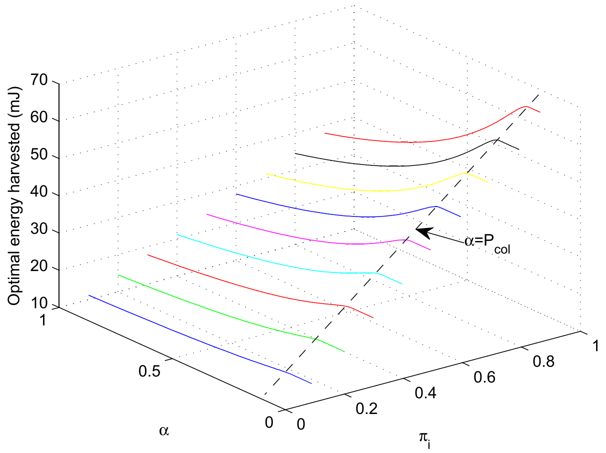

FIGURE 6. The optimal energy harvesting rate vs the probability of channel being idle and the temporal correlation constraint.

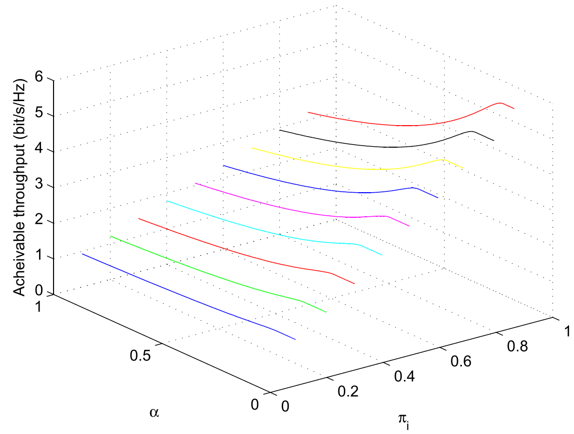

FIGURE 8. The maximum achievable throughput vs the probability of primary channel being idle and the temporal correlation constraint while $e_h = 50mJ$.

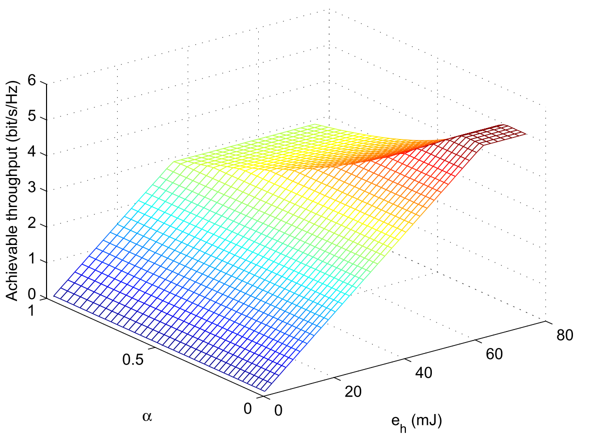

FIGURE 7. The maximum achievable throughput vs the energy harvesting rate and the temporal correlation constraint.

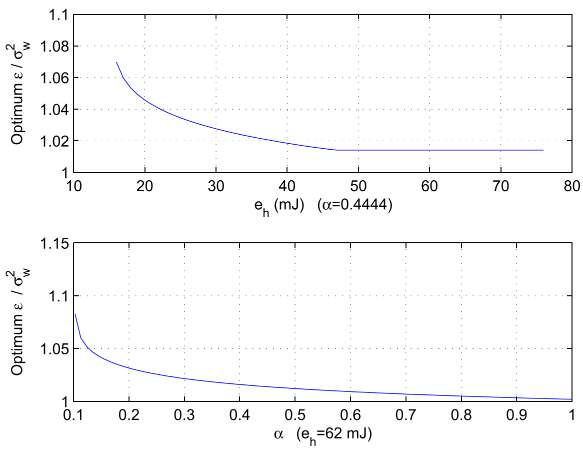

FIGURE 9. Optimal detection threshold vs energy harvesting rate and α.

increases with α decreasing, and $e_{h,opt}$ increases. If $\alpha \leq P_{col}$, $e_{h,1}$ is independent of α and hence, it keeps unchanged.

The maximum achievable throughput versus α and energy harvesting rate is shown in Fig. 7, where e_h changes from 1 mJ to (e_s+e_t) mJ. From the figure, we can see that the throughput increases with the energy harvesting rate until the energy harvesting rate achieves the optimal value, then it will keep unchanged. Besides, the maximum achievable throughput increases with α decreasing, and the energy needed to achieve the maximum throughput increases with α decreasing, which means that more opportunities are available for secondary user to access, meanwhile, more energy is needed to achieve the maximum achievable throughput. The maximum achievable throughput versus α and π_i is also plotted as shown in Fig. 8. It is observed that the maximum achievable throughput increases with π_i increasing while α is fixed, meanwhile the throughput increases with α descending, and keeps unchange while $\alpha < P_{col}$.

The optimal sensing threshold ε versus energy harvesting rate e_h and α is shown in Fig. 9. It is shown that in the upper figure of Fig. 9 the optimum detection threshold decreases as the increasing of energy harvesting rate until the energy harvesting rate reaches the optimal value, then the optimal detection threshold keeps unchanged. As the increasing of energy harvesting rate, more energy can be used by secondary transmitter to operate the data transmission, and the probability of collision with primary user increases. Thus, high detection probability is need, which results into the decreasing of detection threshold until the target collision probability is reached, then the detection threshold keeps unchanged. Besides, there is no optimum detection threshold for low energy harvesting rate when the energy harvesting rate is very low, which is because the limited harvested energy to operate the secondary transmitter is not enough to bring about more collision than the target collision probability.

From the lower plot of Fig. 9, it is seen that the optimum detection threshold decreases as the increasing of α for a given energy arrival rate when $\alpha > P_{col}$, and there is no optimum detection threshold when $\alpha \leq P_{col}$ as we have mentioned above. That is because the probability of primary channel being occupied given secondary transmitter in active state increases with α, then the detection probability should increase in order to keep the target collision probability.

V. CONCLUSION

In this paper, we have considered a cognitive radio network in which the secondary transmitter equipped with an energy harvesting device is allowed to opportunistically access the primary channel. By utilizing the average throughput for the secondary network as a design criterion and jointly optimizing energy harvesting and spectrum sensing, we have achieved both the energy efficiency and the spectrum efficiency. The corresponding optimal detection threshold, energy harvesting rate and the maximum achievable throughput has been obtained under the energy causality and collision constraints. In addition, the effect of target collision probability and the temporal correlation constraint on the achievable throughput has been also discussed. Finally, comprehensive computer simulation results have presented to validate the theoretical analysis and to demonstrate the performance of the proposed maximum achievable throughput and the optimal detection threshold.

APPENDIX A
PROOF OF LEMMA 1

Fixing e_h and ε, the maximization of the objective function (9) can be split into two main conditions $\alpha > P_{col}$ and $\alpha \leq P_{col}$. Then, each condition is further split into several sub-conditions. Taking $\alpha > P_{col}$ for example, three different sub-conditions are shown in Figs. 10, 11 and 12. It is seen that each sub-condition is further split into several small cases for ease to understanding. Note that maximization of $R(P_i,P_o,e_h,\varepsilon)$ for fixed e_h and ε in our work is a problem of linear programming, since the objective and all constraint functions are linear. As a result, the extreme points exist at the intersections of the straight-line boundary segments of the feasible domain [27]. Because the objective is increasing function of P_i and P_o, the maximum $R(P_i,P_o,e_h,\varepsilon)$ achieves at point A (P_i^A, P_o^A) or point B (P_i^B, P_o^B). For ease to recount the proof, we first denote $\Delta = R(P_i^A,P_o^A,e_h,\varepsilon) - R(P_i^B,P_o^B,e_h,\varepsilon)$. If $\Delta < 0$, the maximum $R(P_i,P_o,e_h,\varepsilon)$ achieves at point B, otherwise, it achieves at point A. Specifically, we investigate the maximization problem one case by another case in the sequel. Firstly, we study the condition $\alpha > P_{col}$.

1) $\mu(e_h,\varepsilon) \geq 1$

as shown in Fig. 10. In this case, the feasible domain of (P_i, P_o) changes with the collision constraint:

a: $P_{col}/(1-P_d(\varepsilon)) \geq 1$

As shown in Fig. 10(a),

$$\max_{P_i,P_o} R(P_i,P_o,e_h,\varepsilon)=\Phi_i\big(1-P_f(\varepsilon)\big)+\Phi_o\big(1-P_d(\varepsilon)\big). \quad (13)$$

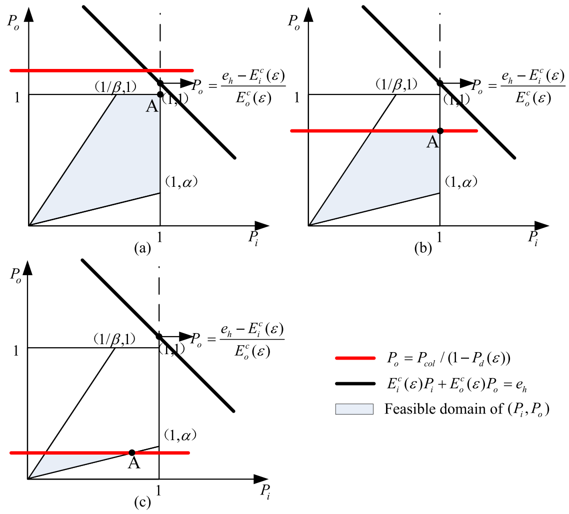

FIGURE 10. Maximization of the secondary throughput with fixed e_h and ε, while $\mu(e_h,\varepsilon) \geq 1$, $\alpha > P_{col}$.

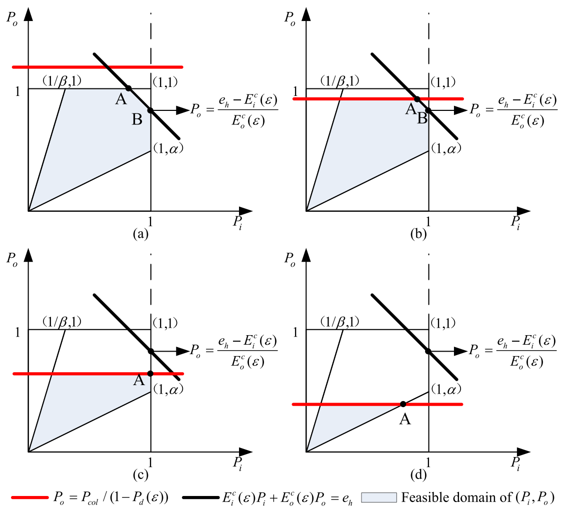

FIGURE 11. Maximization of the secondary throughput with fixed e_h and ε, while $\alpha \leq \mu(e_h,\varepsilon) < 1$, $\alpha > P_{col}$.

b: $\alpha \leq P_{col}/(1-P_d(\varepsilon)) < 1$

As shown in Fig. 10(b),

$$\max_{P_i,P_o} R(P_i,P_o,e_h,\varepsilon) = \Phi_i\big(1-P_f(\varepsilon)\big) + \Phi_o P_{col}. \quad (14)$$

c: $P_{col}/(1-P_d(\varepsilon)) < \alpha$ and $\alpha > P_{col}$

As shown in Fig. 10(c),

$$\max_{P_i,P_o} R(P_i,P_o,e_h,\varepsilon)=\Phi_i\frac{P_{col}\big(1-P_f(\varepsilon)\big)}{\alpha\big(1-P_d(\varepsilon)\big)}+\Phi_o P_{col}. \quad (15)$$

2) $\alpha \leq \mu(e_h,\varepsilon) < 1$

as shown in Fig. 11. In this case, the feasible domain of (P_i, P_o) is split into four sub-conditions on collision constraint:

a: $P_{col}/(1-P_d(\varepsilon)) \geq 1$

As shown in Fig. 11(a). $R(P_i, P_o, e_h, \varepsilon)$ achieves the maximum value at point B, and

$$\max_{P_i,P_o} R(P_i, P_o, e_h, \varepsilon) = \Phi_i\big(1-P_f(\varepsilon)\big) + \Phi_o\mu(e_h,\varepsilon)\big(1-P_d(\varepsilon)\big). \tag{16}$$

Since $\Delta = \frac{T-\tau}{T}\big(e_h - E_i^c(\varepsilon) - E_o^c(\varepsilon)\big)\big(\frac{C_i}{e_s/(1-P_f(\varepsilon))+e_t} - \frac{C_o}{e_s/(1-P_d(\varepsilon))+e_t}\big) < 0$, where $C_i > C_o$, $1-P_f(\varepsilon) > 1-P_d(\varepsilon)$, $e_s/\big(1-P_f(\varepsilon)\big) + e_t < e_s/\big(1-P_d(\varepsilon)\big) + e_t$, $e_h - E_i^c(\varepsilon) - E_o^c(\varepsilon) < 0$.

b: $\mu(e_h,\varepsilon) \leq P_{col}/(1-P_d(\varepsilon)) < 1$

As shown in Fig. 11(b). $R(e_h, \varepsilon)$ obtains the maximum value at point B, and

$$\max_{P_i,P_o} R(P_i,P_o,e_h,\varepsilon) = \Phi_i(1-P_f(\varepsilon)) + \Phi_o\mu(e_h,\varepsilon)(1-P_d(\varepsilon)). \tag{17}$$

Since $\Delta = \frac{T-\tau}{T}\big(e_h - E_i^c(\varepsilon) - E_o^c(\varepsilon)\frac{P_{col}}{1-P_d(\varepsilon)}\big)\big(\frac{C_i}{e_s/(1-P_f(\varepsilon))+e_t} - \frac{C_o}{e_s/(1-P_d(\varepsilon))+e_t}\big) < 0$, where $e_h - E_i^c(\varepsilon) - E_o^c(\varepsilon)\frac{P_{col}}{1-P_d(\varepsilon)} < 0$, $C_i > C_o$, $1-P_f(\varepsilon) > 1-P_d(\varepsilon)$, $e_s/\big(1-P_f(\varepsilon)\big) + e_t < e_s/\big(1-P_d(\varepsilon)\big) + e_t$, $e_h - E_i^c(\varepsilon) - E_o^c(\varepsilon) < 0$.

c: $\alpha \leq P_{col}/(1-P_d(\varepsilon)) < \mu(e_h,\varepsilon)$

As shown in Fig. 11(c),

$$\max_{P_i,P_o} R(P_i, P_o, e_h, \varepsilon) = \Phi_i\big(1-P_f(\varepsilon)\big) + \Phi_o P_{col}. \tag{18}$$

d: $P_{col}/(1-P_d(\varepsilon)) < \alpha$ and $\alpha > P_{col}$

As shown in Fig. 11(d),

$$\max_{P_i,P_o} R(P_i,P_o,e_h,\varepsilon) = \Phi_i\frac{P_{col}\big(1-P_f(\varepsilon)\big)}{\alpha\big(1-P_d(\varepsilon)\big)} + \Phi_o P_{col}. \tag{19}$$

3) $\mu(e_h,\varepsilon) < \alpha$

As shown in Fig. 12. The feasible domain is split into three sub-conditions on the collision constraint:

a: $P_{col}/(1-P_d(\varepsilon)) \geq 1$

As shown in Fig. 12(a), $R(e_h, \varepsilon)$ obtains the maximum value at point B, and

$$\max_{P_i,P_o} R(P_i, P_o, e_h, \varepsilon) = \lambda(e_h,\varepsilon) \times\big(\Phi_i\big(1-P_f(\varepsilon)\big) + \Phi_o\alpha\big(1-P_d(\varepsilon)\big)\big). \tag{20}$$

Since $\Delta = \frac{T-\tau}{T}\frac{\alpha e_h - E_i^c(\varepsilon) - \alpha E_o^c(\varepsilon)}{E_i^c(\varepsilon)\big(E_i^c(\varepsilon)+\alpha E_o^c(\varepsilon)\big)}\big(1-P_d(\varepsilon)\big)\big(1-P_f(\varepsilon)\big)\pi_i\pi_o\big(C_i\big(\frac{e_s}{1-P_d(\varepsilon)}+e_t\big) - C_o\big(\frac{e_s}{1-P_f(\varepsilon)}+e_t\big)\big) < 0$, where $C_i > C_o$, $1-P_d(\varepsilon) < 1-P_f(\varepsilon)$, $\alpha e_h - E_i^c(\varepsilon) - \alpha E_o^c(\varepsilon) < 0$.

b: $\alpha\lambda(e_h,\varepsilon) \leq P_{col}/(1-P_d(\varepsilon)) < 1$

As shown in Fig. 12(b), $R(e_h, \varepsilon)$ obtains the maximum value at point B, and

$$\max_{P_i,P_o} R(P_i, P_o, e_h, \varepsilon) = \lambda(e_h,\varepsilon) \times\big(\Phi_i\big(1-P_f(\varepsilon)\big) + \Phi_o\alpha\big(1-P_d(\varepsilon)\big)\big). \tag{21}$$

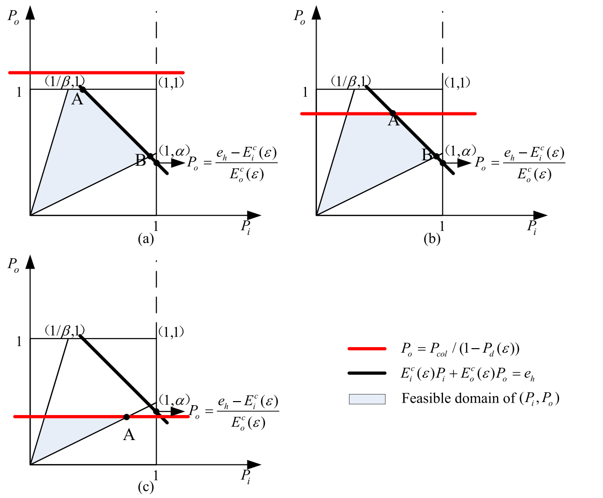

FIGURE 12. Maximization of the secondary throughput with fixed e_h and ε, while $(e_h - E_i^c(\varepsilon))/E_o^c(\varepsilon) < \alpha$, $\alpha > P_{col}$.

Since $\Delta = \frac{\alpha e_h - (E_i^c(\varepsilon)+\alpha E_o^c(\varepsilon))\frac{P_{col}}{1-P_d(\varepsilon)}}{E_i^c(\varepsilon)(E_i^c(\varepsilon)+\alpha E_o^c(\varepsilon))}\big(\Phi_i\big(1-P_f(\varepsilon)\big)E_o^c(\varepsilon) - \Phi_o\big(1-P_d(\varepsilon)\big)E_i^c(\varepsilon)\big) < 0$, where $\alpha e_h - (E_i^c(\varepsilon)+\alpha E_o^c(\varepsilon))\frac{P_{col}}{1-P_d(\varepsilon)} < 0$, $\Phi_i\big(1-P_f(\varepsilon)\big)E_o^c(\varepsilon) - \Phi_o\big(1-P_d(\varepsilon)\big)E_i^c(\varepsilon) > 0$.

c: $P_{col}/(1-P_d(\varepsilon)) < \alpha\lambda(e_h,\varepsilon)$ and $\alpha > P_{col}$

As shown in Fig. 12(c),

$$\max_{P_i,P_o} R(e_h, \varepsilon) = \Phi_i\frac{P_{col}\big(1-P_f(\varepsilon)\big)}{\alpha\big(1-P_d(\varepsilon)\big)} + \Phi_o P_{col}. \tag{22}$$

Consequently, 1) Feasible set (e_h, ε) of (13) is denoted by Ω_1; 2) Feasible set (e_h, ε) of (14) and (18) are combined into Ω_2; 3) Feasible set (e_h, ε) of (15), (19) and (18) are combined into Ω_3; 4) Feasible set (e_h, ε) of (16) and (17) are combined into Ω_4; 5) Feasible set (e_h, ε) of (16) and (17) are combined into Ω_5.

On the other hand, if $\alpha \leq P_{col}$, (15), (19) and (18) do not exist, and thus, Ω_3 is empty. Meanwhile Ω_2 and Ω_5 change to $\bar{\Omega}_2$ and $\bar{\Omega}_5$, respectively. This completes the proof of Lemma 1. □

APPENDIX B
PROOF OF LEMMA 2

The first order derivative of $F(\varepsilon)$ is given by

$$F'(\varepsilon) = \frac{\tau f\sigma_p^2}{\sigma_w^4}\left(\frac{\sigma_p^2 + 2\sigma_w^2}{\sigma_w^2(\sigma_w^2+\sigma_p^2)}\varepsilon - 1\right)\Xi,$$

where $\Xi = \big(1-P_d(\varepsilon)\big)\exp\left(-\frac{\tau f}{2}\left(\frac{(\varepsilon-\sigma_w^2)^2}{\sigma_w^4} - \frac{(\varepsilon-\sigma_w^2-\sigma_p^2)^2}{(\sigma_w^2+\sigma_p^2)^2}\right)\right)$. Letting $F'(\varepsilon) = 0$ yields $\varepsilon = \bar{\varepsilon} = \frac{\sigma_w^2(\sigma_w^2+\sigma_p^2)}{\sigma_p^2+2\sigma_w^2}$. In addition, we have $F'(\varepsilon) > 0$ when $\varepsilon > \bar{\varepsilon}$, and $F'(\varepsilon) < 0$ when $\varepsilon < \bar{\varepsilon}$. Thus, $F(\varepsilon)$ is an increasing function of ε in $(\bar{\varepsilon}, \infty)$ and a decreasing function of ε in $(0, \bar{\varepsilon})$. As a consequence, $F(\varepsilon)$ achieves its minimum value at $\varepsilon = \bar{\varepsilon}$ and $F(\bar{\varepsilon}) < 0$. Since $\lim_{\varepsilon\to 0} F(\varepsilon) \to 0$ and $\lim_{\varepsilon\to\infty} F(\varepsilon) \to 1$, there is only one

$\varepsilon = \tilde{\varepsilon} > \bar{\varepsilon}$ satisfying $F(\tilde{\varepsilon}) = 0$. Therefore, we obtain that $F(\varepsilon) < 0$ when $\varepsilon < \tilde{\varepsilon}$, and $F(\varepsilon) > 0$ when $\varepsilon > \tilde{\varepsilon}$. On the other hand, if we let $G(\varepsilon) = P'_d(\varepsilon) - P'_d(\varepsilon)$, there must be one $\dot{\varepsilon} \in (\sigma_w^2, \sigma_w^2 + \sigma_p^2)$ that satisfies $G(\dot{\varepsilon}) = 0$, since $G(\sigma_w^2 + \sigma_p^2) > 0 > G(\sigma_w^2)$. In other words, there must be one $\dot{\varepsilon} \in (\sigma_w^2, \sigma_w^2 + \sigma_p^2)$ such that $P'_d(\dot{\varepsilon}) = P'_f(\dot{\varepsilon})$. Therefore, we have $F(\dot{\varepsilon}) = P_d(\dot{\varepsilon}) - P_f(\dot{\varepsilon}) > 0$. In addition to $\bar{\varepsilon} < \tilde{\varepsilon} < \dot{\varepsilon}$, we obtain that there is a $\tilde{\varepsilon} \in (\bar{\varepsilon}, \sigma_w^2 + \sigma_p^2)$ that satisfies $F(\tilde{\varepsilon}) = 0$. This completes the proof of Lemma 2. □

APPENDIX C
PROOF OF THEOREM 1

Let us first consider the case when $\alpha > P_{col}$. Note that $R(e_h, \varepsilon)$ increases with e_h increasing in Ω_4 and Ω_5, since $\mu(e_h, \varepsilon)$ and $\lambda(e_h, \varepsilon)$ are both increasing functions of e_h. In addition, $R(e_h, \varepsilon)$ is independent of e_h in the feasible domains Ω_1, Ω_2 and Ω_3, and $R(e_h, \varepsilon)$ is continuous on the edge of each domain. Therefore, $R(e_h, \varepsilon)$ achieves maximum with respect to e_h in Ω_1, Ω_2 or Ω_3. We also notice that $R(e_h, \varepsilon)$ increases with ε increasing in Ω_1 and Ω_2, since $P_d(\varepsilon)$ and $P_f(\varepsilon)$ are both decreasing functions of ε. Then, it can be further obtained that $R(e_h, \varepsilon)$ achieves maximum with respect to ε in Ω_3. Notice that in Ω_3, we have $\varepsilon \geq \varepsilon_1$, where $\varepsilon_1 = (\mathcal{Q}^{-1}(1 - \frac{P_{col}}{\alpha})/\sqrt{\tau f} + 1)(\sigma_w^2 + \sigma_p^2)$, with $\mathcal{Q}^{-1}(x)$ being the inverse of $\mathcal{Q}$-function. Since $\mathcal{Q}^{-1}(1 - \frac{P_{col}}{\alpha})/\sqrt{\tau f} \approx 0$ when τf is large enough, we have $\varepsilon_1 \approx \sigma_w^2 + \sigma_p^2$ and thus, $\varepsilon_1 \geq \tilde{\varepsilon}$. If we let $f(\varepsilon) = (1 - P_f(\varepsilon))/(1 - P_d(\varepsilon))$, then, the first order derivative of $f(\varepsilon)$ is given by $f'(\varepsilon) = P'_d(\varepsilon)F(\varepsilon)/\big(1 - P_d(\varepsilon)\big)^2$. Using Lemma 2 and $P'_d(\varepsilon) < 0$, we arrive at the fact that $f'(\varepsilon) < 0$ for $\varepsilon > \varepsilon_1$. Hence, the maximum $R(e_h, \varepsilon)$ achieves at $\varepsilon_{opt} = \varepsilon_1$. The optimal e_h is at the intersection of Ω_2, Ω_3, Ω_4 and Ω_5.

Similarly, when $\alpha \leq P_{col}$, we can prove that $R(e_h, \varepsilon)$ is increasing in terms of e_h in Ω_4 and $\bar{\Omega}_5$ and is independent of e_h in Ω_1 and $\bar{\Omega}_2$. In addition, $R(e_h, \varepsilon)$ is continuous on the edge of each domain, and $R(e_h, \varepsilon)$ increases with respect to ε in Ω_1 and $\bar{\Omega}_2$. Therefore, the limit of $R(e_h, \varepsilon)$ with respect to e_h and ε lies in $\bar{\Omega}_2$. Since $P_f(\varepsilon) > 0$, $R(e_h, \varepsilon) < \Phi_i + \Phi_o P_{col}$. Furthermore, $\lim_{\varepsilon\to\infty} P_f(\varepsilon) = 0$, and $\lim_{\varepsilon\to\infty} R(1, P_{col}, e_h, \varepsilon) = \Phi_i + \Phi_o P_{col}$ for any $e_h \geq e_{h,1} = \lim_{\varepsilon\to\infty} \frac{P_{col}}{1-P_d(\varepsilon)} E_o^c(\varepsilon) + E_i^c(\varepsilon) = (e_s + e_t)(\pi_i + P_{col}\pi_o)$. This completes the proof of Theorem 1 □.

APPENDIX D
PROOF OF THEOREM 2

Let us firstly deal with the situation where $\alpha > P_{col}$. As we have proved that $R(e_h, \varepsilon)$ increases with ε increasing in Ω_1 and Ω_2, decreases with ε increasing in Ω_3, and increases with e_h increasing in Ω_4 and Ω_5, we need only to investigate the monotonicity of $R(e_h, \varepsilon)$ on ε in Ω_4 and Ω_5 to obtain the maximum $R(e_h, \varepsilon)$.

In Ω_4, the first order derivative of $R(e_h, \varepsilon)$ with respect to ε in Ω_4 is given by $\frac{\partial R(e_h,\varepsilon)}{\partial \varepsilon} = \big(-P'_f(\varepsilon)E_o^c(\varepsilon)\Psi - \Phi_o\big(e_h - E_i^c(\varepsilon)\big)P'_d(\varepsilon)e_s\pi_o\big)/E_o^c(\varepsilon)^2$, where $\Psi = \Phi_i e_s \pi_o + \big(1 - P_d(\varepsilon)\big)e_t(\Phi_i\pi_o - \Phi_o\pi_i)$. Since $\Phi_i\pi_o - \Phi_o\pi_i = \frac{T-\tau}{T}\pi_i\pi_o(C_i - C_o)$, $C_i > C_o$ and $\Phi_i\pi_o - \Phi_o\pi_i > 0$, we obtain $\Psi > 0$, meanwhile, we also obtain $e_h - E_i^c(\varepsilon) > 0$ due to $\mu(e_h, \varepsilon) > \alpha$ in Ω_4, In addition to $P'_f(\varepsilon) < 0$ and $P'_d(\varepsilon) < 0$, we obtain that $\frac{\partial R(e_h,\varepsilon)}{\partial \varepsilon} > 0$ and thus, $R(e_h, \varepsilon)$ is an increasing function of ε in Ω_4. As a consequence, the maximum throughput in Ω_4 is obtained on the boundary.

In Ω_5, the first order derivative of $R(e_h, \varepsilon)$ with respect to ε is given by $\frac{\partial R(e_h,\varepsilon)}{\partial \varepsilon} = \frac{-e_h G(\varepsilon)}{(E_i^c(\varepsilon)+\alpha E_o^c(\varepsilon))^2}$, where $G(\varepsilon) = e_s(\pi_i + \alpha\pi_o)\big(P'_f(\varepsilon)\Phi_i + P'_d(\varepsilon)\alpha\Phi_o\big) - \alpha e_t(\Phi_i\pi_o - \Phi_o\pi_i)P'_d(\varepsilon)F(\varepsilon)$. Since the primary signal SNR is low, we consider $C_i \approx C_o$ and then, $\Phi_i\pi_o - \Phi_o\pi_i = \frac{T-\tau}{T}\pi_i\pi_o(C_i - C_o) \approx 0$. Therefore, we have $G(\varepsilon) \approx e_s(\pi_i + \alpha\pi_o)\big(P'_f(\varepsilon)\Phi_i + P'_d(\varepsilon)\alpha\Phi_o\big) < 0$, because of the fact that $P'_d(\varepsilon)$ and $P'_f(\varepsilon)$ are negative and other variables are all positive. Hence, we obtain $\frac{\partial R(e_h,\varepsilon)}{\partial \varepsilon} > 0$ and as a result, $R(e_h, \varepsilon)$ is an increasing function of ε in Ω_5.

From Fig. 2, we can see that Ω_5 can be further split into two sub-conditions on e_h :1) $e_h \leq e_{h,3}$, 2) $e_{h,3} \leq e_h < e_{h,opt}$, where $e_{h,3} = (e_s + e_t)(\pi_i + \alpha\pi_o)P_{col}/\alpha$ is the energy value at the edge between Ω_4 and Ω_5 with $\varepsilon \to \infty$.

1) When the harvested energy $e_h \leq e_{h,3}$, the limit of the achievable throughput is given by

$$\lim_{\varepsilon\to\infty} R(e_h, \varepsilon) = \frac{e_h(\Phi_i + \alpha\Phi_o)}{(e_s + e_t)(\pi_i + \alpha\pi_o)}. \tag{23}$$

Consequently, there is no optimum detection threshold for this condition.

2) When the harvested energy $e_{h,3} \leq e_h < e_{h,opt}$, the achievable throughput reaches the maximum at the edge between Ω_3 and Ω_5, where $\lambda(e_h, \varepsilon) = \frac{P_{col}}{\alpha(1-P_d(\varepsilon))}$. Let $Y(\varepsilon) = \lambda(e_h, \varepsilon) - \frac{P_{col}}{\alpha\big(1-P_d(\varepsilon)\big)}$. Then, $\varepsilon_{opt,2} = Y^{-1}(0)$ is the optimum detection threshold for given e_h, and

$$\max_{\varepsilon} R(e_h, \varepsilon) = \Phi_i \frac{P_{col}\big(1 - P_f(\varepsilon_{opt,2})\big)}{\alpha\big(1 - P_d(\varepsilon_{opt,2})\big)} + \Phi_o P_{col}. \tag{24}$$

In addition to $R(e_h, \varepsilon)$ is continuous at the edge of adjacent two feasible sets, the maximum achievable throughput with $e_h < e_{h,opt}$ is expressed as (23) and (24) when $P_{col} < \alpha$.

Now, let us consider the case when $\alpha \leq P_{col}$. Just as we have proved above, $R(e_h, \varepsilon)$ is an increasing function of ε in Ω_4 and $\bar{\Omega}_5$. If $e_{h,2} \leq e_h < e_{h,1}$, where $e_{h,2} = (e_s + e_t)(\pi_i + \alpha\pi_o)$ is the energy value at the edge between Ω_4 and $\bar{\Omega}_5$ as shown in Fig. 3, then, the limit of the throughput in Ω_4 is determined by

$$\lim_{\varepsilon\to\infty} R(e_h, \varepsilon) = \Phi_i + \Phi_o\bigg(\frac{e_h}{(e_s + e_t)\pi_o} - \frac{\pi_i}{\pi_o}\bigg). \tag{25}$$

If $e_h < e_{h,2}$, since the throughput in Ω_4 and $\bar{\Omega}_5$ increases with ε for the given e_h, and the throughput at the edge between Ω_4 and $\bar{\Omega}_5$ is continuous, the limit of the throughput in $\bar{\Omega}_5$ is determined by

$$\lim_{\varepsilon \to \infty} R(e_h, \varepsilon) = \frac{e_h(\Phi_i + \alpha \Phi_o)}{(e_s + e_t)(\pi_i + \alpha \pi_o)}. \quad (26)$$

Therefore, there is no optimum detection threshold under these two conditions. This completes the proof of Theorem 2. □

Acknowledgment

This work is performed while Han is a visiting Ph.D. student in McMaster University.

REFERENCES

[1] L. X. Cai, H. V. Poor, Y. Liu, T. H. Luan, X. Shen, and J. W. Mark, "Dimensioning network deployment and resource management in green mesh networks," *IEEE Wireless Commun.*, vol. 18, no. 5, pp. 58–65, Oct. 2011.

[2] X. Lu, P. Wang, D. Niyato, D. I. Kim, and Z. Han, "Wireless networks with RF energy harvesting: A contemporary survey," *IEEE Commun. Surveys Tut.*, vol. 17, no. 2, pp. 757–789, 2nd Quart., 2015.

[3] K. Huang, "Spatial throughput of mobile ad hoc networks powered by energy harvesting," *IEEE Trans. Inf. Theory*, vol. 59, no. 11, pp. 7597–7612, Nov. 2013.

[4] X. Huang, T. Han, and N. Ansari, "On green energy powered cognitive radio networks," *IEEE Commun. Surveys Tut.*, vol. 17, no. 2, pp. 827–842, 2nd Quart., 2015.

[5] S. Haykin, "Cognitive radio: Brain-empowered wireless communications," *IEEE J. Sel. Areas Commun.*, vol. 23, no. 2, pp. 201–220, Feb. 2005.

[6] T. Yucek and H. Arslan, "A survey of spectrum sensing algorithms for cognitive radio applications," *IEEE Commun. Surveys Tut.*, vol. 11, no. 1, pp. 116–130, 1st Quart., 2009.

[7] R. Deng, J. Chen, C. Yuen, P. Cheng, and Y. Sun, "Energy-efficient cooperative spectrum sensing by optimal scheduling in sensor-aided cognitive radio networks," *IEEE Trans. Veh. Technol.*, vol. 61, no. 2, pp. 716–725, Feb. 2012.

[8] E. C. Y. Peh, Y.-C. Liang, Y. L. Guan, and Y. Zeng, "Cooperative spectrum sensing in cognitive radio networks with weighted decision fusion schemes," *IEEE Trans. Wireless Commun.*, vol. 9, no. 12, pp. 3838–3847, Dec. 2010.

[9] S. Lee and R. Zhang, "Cognitive wireless powered network: Spectrum sharing models and throughput maximization," *IEEE Trans. Cogn. Commun. Netw.*, vol. 1, no. 3, pp. 335–346, Sep. 2015.

[10] C. Yang, J. Li, M. Guizani, A. Anpalagan, and M. Elkashlan, "Advanced spectrum sharing in 5G cognitive heterogeneous networks," *IEEE Wireless Commun.*, vol. 23, no. 2, pp. 94–101, Apr. 2016.

[11] X. Lu, P. Wang, D. Niyato, and K. Hossain, "Dynamic spectrum access in cognitive radio networks with RF energy harvesting," *IEEE Wireless Commun.*, vol. 21, no. 3, pp. 102–110, Jun. 2014.

[12] S. Lee, R. Zhang, and K. Huang, "Opportunistic wireless energy harvesting in cognitive radio networks," *IEEE Trans. Wireless Commun.*, vol. 12, no. 9, pp. 4788–4799, Sep. 2013.

[13] F. Yuan, Q. T. Zhang, S. Jin, and H. Zhu, "Optimal harvest-use-store strategy for energy harvesting wireless systems," *IEEE Trans. Wireless Commun.*, vol. 14, no. 2, pp. 698–710, Feb. 2015.

[14] M.-L. Ku, W. Li, Y. Chen, and K. J. R. Liu, "Advances in energy harvesting communications: Past, present, and future challenges," *IEEE Commun. Surveys Tut.*, vol. 18, no. 2, pp. 1384–1412, 2nd Quart., 2016.

[15] N. Pappas, J. Jeon, A. Ephremides, and A. Traganitis, "Optimal utilization of a cognitive shared channel with a rechargeable primary source node," *J. Commun. Netw.*, vol. 14, no. 2, pp. 162–168, Apr. 2012.

[16] A. Sultan, "Sensing and transmit energy optimization for an energy harvesting cognitive radio," *IEEE Wireless Commun. Lett.*, vol. 1, no. 5, pp. 500–503, Oct. 2012.

[17] S. Park, H. Kim, and D. Hong, "Cognitive radio networks with energy harvesting," *IEEE Trans. Wireless Commun.*, vol. 12, no. 3, pp. 1386–1397, Mar. 2013.

[18] S. Park and D. Hong, "Optimal spectrum access for energy harvesting cognitive radio networks," *IEEE Trans. Wireless Commun.*, vol. 12, no. 12, pp. 6166–6179, Dec. 2013.

[19] W. Chung, S. Park, S. Lim, and D. Hong, "Spectrum sensing optimization for energy-harvesting cognitive radio systems," *IEEE Trans. Wireless Commun.*, vol. 13, no. 5, pp. 2601–2613, May 2014.

[20] S. Park and D. Hong, "Achievable throughput of energy harvesting cognitive radio networks," *IEEE Trans. Wireless Commun.*, vol. 13, no. 2, pp. 1010–1022, Feb. 2014.

[21] H. S. Dhillon, Y. Li, P. Nuggehalli, Z. Pi, and J. G. Andrews, "Fundamentals of heterogeneous cellular networks with energy harvesting," *IEEE Trans. Wireless Commun.*, vol. 13, no. 5, pp. 2782–2797, May 2014.

[22] D. Niyato, P. Wang, and D. I. Kim, "Channel selection in cognitive radio networks with opportunistic RF energy harvesting," in *Proc. IEEE Int. Conf. Commun. (ICC)*, Sydney, NSW, Australia, Jun. 2014, pp. 1555–1560.

[23] S. Yin, E. Zhang, L. Yin, and S. Li, "Optimal saving-sensing-transmitting structure in self-powered cognitive radio systems with wireless energy harvesting," in *Proc. IEEE Int. Conf. Commun. (ICC)*, Budapest, Hungary, Jun. 2013, pp. 2807–2811.

[24] X. Gao, W. Xu, S. Li, and J. Lin, "An Online energy allocation strategy for energy harvesting cognitive radio systems," in *Proc. Int. Conf. Wireless Commun. Signal Process. (WCSP)*, Hangzhou, China, Oct. 2013, pp. 1–5.

[25] Y.-C. Liang, Y. Zeng, E. C. Y. Peh, and A. T. Hoang, "Sensing-throughput tradeoff for cognitive radio networks," *IEEE Trans. Wireless Commun.*, vol. 7, no. 4, pp. 1326–1337, Apr. 2008.

[26] S. Cui, A. J. Goldsmith, and A. Bahai, "Energy-constrained modulation optimization," *IEEE Trans. Wireless Commun.*, vol. 4, no. 5, pp. 2349–2360, Sep. 2005.

[27] S. Boyd and L. Vandenberghe, *Convex optimization*. Cambridge, U.K.: Cambridge Univ. Press, 2004.

GANGTAO HAN received the B.E. degree from the School of Information Engineering, Zhengzhou University, Zhengzhou, China, in 2008, where he is currently pursuing the Ph.D. degree. From 2014 to 2016, he was a Visiting Student with the Department of Electronic and Computer Engineering, McMaster University, ON, Canada. His research interests include wireless communications, cognitive radio, and signal processing in massive MIMO.

JIAN-KANG ZHANG (SM'09) received the B.S. degree in information science (mathematics) from Shaanxi Normal University, Xi'an, China, the M.S. degree in information and computational science (mathematics) from Northwest University, Xi'an, and the Ph.D. degree in electrical engineering from Xidian University, Xi'an. He has held a research positions with Harvard University and McMaster University. He is currently an Associate Professor with the Department of Electrical and Computer Engineering, McMaster University. His research interests include massive MIMO, visible light communication, cognitive radio, signal detection, and estimation. He has co-authored the paper that received the IEEE Signal Processing Society Best Young Author Award in 2008. He has served as an Associate Editor of the IEEE Transactions on Signal Processing and the IEEE Signal Processing Letters. He is currently serving as an Associate Editor of the *Journal of Electrical and Computer Engineering*.

XIAOMIN MU received the B.E. degree from the Beijing Institute of Technology, Beijing, China, in 1982. She is currently a Full Professor with the School of Information Engineering, Zhengzhou University. She has authored many papers in the field of signal processing and co-authored two books. Her research interests include signal processing in communication systems, wireless communications, and cognitive radio.